

Possible cluster in the Galactic center

Martínez Arranz, Á¹ and Schödel, R²

¹ Instituto de Astrofísica de Andalucía, Glorieta de la astronomía, Granada, Spain
e-mail: amatinez@iaa.csic.es

² yomama

Received xx / Accepted xx

ABSTRACT

Context. This is the context.

Aims. This is what the study aims to explore.

Methods. This is how it was done.

Results. These are the results.

Conclusions. These are the conclusions.

Key words. Galaxy: center – stars: formation – proper motions – catalogs – surveys

1. Introduction

- Other catalogs are shallow
- Other catalogs do not cover enough area in the NSD
- Other catalogs do not have enough precision
- Top-heavy IMF in Arches and Quintuple? Is this a consequence of this extreme environment? We need more cluster to study?
- Top-heavy IMF in Arches and Quintuple? Is this a consequence of this extreme environment? We need more cluster to study?
- we present the first results of the GNS proper motion catalog

Located at a distance of ~ 8.2 kpc from Earth (GRAVITY Collaboration et al. 2020), the Galactic Center (GC) hosts the Nuclear Stellar Disk (NSD), a flat, rotating structure approximately 150–200 pc across and 40–50 pc in scale height (Launhardt et al. 2002a; Schonrich et al. 2015; Shahzamanian et al. 2022; Gallego-Cano et al. 2020; Sormani et al. 2022). Despite its small volume—less than 1% of the Galaxy—the NSD is among the most active star-forming regions in the Milky Way, emitting about 10% of the total Lyman continuum flux (Launhardt et al. 2002b; Nishiyama et al. 2008; Morris & Serabyn 1996).

The bulk of the NSD's stellar population is old, with ages $\gtrsim 8$ Gyr (Nogueras-Lara et al. 2020). However, multiple lines of evidence suggest intense and recent star formation episodes within the past 30 Myr, with estimated star formation rates between 0.2 and $0.8 M_{\odot}/\text{yr}$ (Matsunaga et al. 2011; Nogueras-Lara et al. 2020), corresponding to a total stellar mass of approximately $10^6 M_{\odot}$ formed during this period.

Despite evidence for intense star formation in the NSD over the past 30 Myr, the observed young stellar population remains surprisingly sparse. The only known young stellar clusters in the region—the Arches and Quintuplet—each have estimated masses of about $\sim 10^4 M_{\odot}$ (Bartko et al. 2010; Lu et al. 2013). In addition, young and apparently isolated massive stars are found scattered throughout the central 100 pc (e.g. Dong et al. 2011; Cano-González et al. 2021; Clark et al. 2023).

Recent luminosity function analyses have also revealed up to $\sim 10^5 M_{\odot}$ of ~ 10 Myr-old stars in the Sgr B1 and Sgr C regions (Nogueras-Lara et al. 2022; Nogueras-Lara 2024). However, the combined mass of all these young stars still falls short of accounting for the $\sim 10^6 M_{\odot}$ expected from the estimated star formation rate. This discrepancy is known as the *missing cluster problem*.

The disparity between expected and found young stellar populations is likely due to the unique and extreme environment of the GC. High stellar surface densities make it difficult to detect stellar overdensities, especially once clusters begin dissolving. In addition, the strong and variable interstellar extinction in the GC, which limits observations to the near-infrared (?Nogueras-Lara et al. 2019b), prevents accurate photometric separation of young hot stars from old red giants and makes traditional color-magnitude diagram (CMD) analysis ineffective to identify stellar clusters, as the diagrams are heavily affected by reddening and differential extinction (Nogueras-Lara et al. 2018) **cite your thesis**. Moreover, tidal forces and shocks in the GC can dissolve even massive clusters like the Arches within $\lesssim 10$ Myr (Portegies Zwart et al. 2001; Kruijssen et al. 2014), blending them into the stellar background and rendering them undetectable through conventional methods.

Spectroscopy can help identify massive young stars (MYSs) via key spectral features in the near-infrared, such as the absence of CO bandhead absorption and the presence of Bry or He I lines (Paumard et al. 2006; Habibi et al. 2019; Martínez-Arranz et al. 2024b). However, spectroscopy requires high angular resolution and covers limited fields of view, making full surveys of the NSD prohibitively time-consuming.

An alternative method is to identify co-moving group, associations of stars sharing similar positions and velocities and exhibit smaller velocity dispersions than the field stars. In (Martínez-Arranz et al. 2024a) we presented a technique to detect co-moving groups in this crowded and highly extinguished region and found three different co-moving groups with known massive young stars. We confirm through spectroscopic data that partially overlap one of these three groups, that several of its member

were massive young stars (Martínez-Arranz et al. 2024b) confirming the cluster nature of it.

In the aforementioned study we were limited for the extension of the proper motion catalog we have to our disposal Libralato et al. (2021), which covered a relatively small part of the NSD. In the present study we use the much larger **GNS PM CATALOG (REF NEED IT)**, covering a larger portion of the NSD, including several areas of intense HII emission, the smoking gun of recent star formation. In the present case we focus in Sgr-B1 region.

Based on the DBSCAN clustering algorithm (?), our tool searches for over-densities in a five-dimensional parameter space, position, proper motion, and relative line-of-sight distance. For the later, we use color as a proxy. Given the relatively uniform intrinsic colors of GC stars (with $H-K_s$ variation $\lesssim 0.01$ mag) and the large extinction variation (Nogueras-Lara et al. 2018, 2021; Shahzamanian et al. 2022; Nogueras-Lara 2022), color differences are attributed mainly to extinction, and hence can serve as proxies for depth along the line of sight (Nogueras-Lara 2022). For more details, please refer to n (Martínez-Arranz et al. 2024a)

The Galactic Center (GC), located at a distance of approximately ~ 8.25 kpc (GRAVITY Collaboration et al. 2020), hosts the Nuclear Stellar Disk (NSD)—a flattened, rotating structure spanning about 150 pc in diameter and with a scale height of ~ 40 pc (Schonrich et al. 2015; Shahzamanian et al. 2022; Launhardt et al. 2002a; Sormani et al. 2022). Matsunaga et al. (2011) identified three classical Cepheids within the inner projected 40 pc of the GC. This discovery suggests the formation of about $10^6 M_\odot$ of stars in this region over the past ~ 10 Myr, a finding that aligns with the star formation history reported by Nogueras-Lara et al. (2020). With a star formation rate of $[0.2-0.8] M_\odot/\text{yr}$ over the past 30 Myr (Matsunaga et al. 2011; Nogueras-Lara et al. 2020), the NSD stands out as the most prolific star-forming region in the Galaxy when averaged by volume. This high star formation rate, however, contrasts with the small number of known young clusters in the NSD—the Arches and Quintuplet clusters—which together contribute only a small fraction of the inferred stellar mass. This discrepancy, known as the “missing clusters problem,” is not entirely unexpected. The GC’s extreme conditions complicate the detection of young clusters. High and spatially variable extinction (?Nogueras-Lara et al. 2019b) restricts observations to the near-infrared, while strong tidal fields and shocks can dissolve even massive clusters (up to $\sim 10^4 M_\odot$) within 10 Myr (Portegies Zwart et al. 2001; Kruijssen et al. 2014), blending them into the stellar background and hindering their detection through overdensities. These limitations also affect the effectiveness of color-magnitude diagrams (CMDs), which are dominated by reddening and offer little insight into stars’ intrinsic colors (Nogueras-Lara et al. 2018). Nonetheless, recent work has revealed a significant young stellar population—on the order of several $10^5 M_\odot$ —in regions like Sgr B1 and Sgr C by analyzing luminosity functions (Nogueras-Lara et al. 2022; Nogueras-Lara 2024), supporting the scenario of coeval formation followed by rapid dissolution. While spectroscopy offers a path to identifying young stellar associations, it is often constrained by its limited field of view and the high angular resolution required. Thus, a full spectroscopic survey of the NSD would be prohibitively time-consuming. Instead, a more efficient approach involves first identifying potential co-moving groups of stars (e.g., Shahzamanian et al. 2019; Martínez-Arranz et al. 2024a), and then targeting these regions with spectroscopy to confirm the presence of young, massive stars and character-

ize the group. Co-moving groups are collections of stars that are close in space and share similar velocities, with a velocity dispersion smaller than the surrounding field population. These groups can be characterized in six dimensions: three spatial coordinates and three velocity components. While current GC catalogs provide only positions and proper motions in the plane of the sky, the third spatial dimension—line-of-sight distance—can be approximated through stellar colors. Due to the strong and variable extinction in the NSD (Nogueras-Lara et al. 2021; Shahzamanian et al. 2022; Nogueras-Lara 2022) and the nearly constant intrinsic colors of most stars (with $H-K_s$ variations $\lesssim 0.01$ mag; Nogueras-Lara et al. 2018, see Fig. 33), color differences are largely attributed to extinction. Hence, stars with similar colors likely lie at similar depths within the NSD (Nogueras-Lara 2022). If a co-moving group is a remnant of a dissolving cluster or association, its stars should be relatively young (ages $\lesssim 10$ Myr). Young, massive stars (MYSs) can be distinguished from cool, late-type stars using near-infrared spectral lines such as CO and Bry (Paumard et al. 2006; Habibi et al. 2019). Cool stars exhibit ^{12}CO bandhead absorptions at 2.30, 2.33, and $2.35 \mu\text{m}$, whereas MYSs lack these features and may show Bry emission or absorption at $2.16 \mu\text{m}$ and/or HeI absorption at $2.06 \mu\text{m}$. A candidate co-moving group was identified in Shahzamanian et al. (2019), located in an HII-emitting region (?) with a strong Paschen- α emitting star (?Dong et al. 2011), making it a promising site for hosting MYSs. We conducted spectroscopic observations of this area and analyzed the spectra of stars near the center of the group, selecting MYSs based on spectral features. We then cross-matched these stars with the GALACTICNUCLEUS survey (Nogueras-Lara et al. 2018, 2019a) and the proper motion catalog from Libralato et al. (2021), obtaining both photometry and proper motion data.

2. Methods

- Regular reduction with sky observatio
- Photometry with holography
- Astrometry with SCAMP and SExtractor

2.1. GALACTICNUCLEUS survey

In order to compute proper motions we combined two different epoch of GALACTICNUCLEUS survey (GNS), spaced approximately seven years.

The GNS catalog (Nogueras-Lara et al. 2019a, hereafter GNS I) was acquired with the wide-field near-infrared camera HAWK-I/VLT, with fast photometry mode and reduced with the speckle holography algorithm (Schödel et al. 2013) to provide a high homogeneous angular resolution of $0.2''$. The survey covered an area of about $\sim 6000 \text{ pc}^2$ (see Fig. 1) and provide accurate photometry for about $\sim 3.3 \times 10^6$ stars in the J, H and K_s bands, with an uncertainty of $\lesssim 0.05$ mag in all three bands. Due to the extreme crowdedness of this environment sky background was estimated using dithered exposures of a dark cloud region near the Galactic Center ($\alpha \approx 17^\text{h}48^\text{m}01.55^\text{s}$, $\delta \approx -28^\circ59'20''$), characterized by low stellar density. For further details about the reduction process, please refer to Nogueras-Lara et al. (2018, 2019a)

In 2022, seven years after GNS I, a second epoch of imaging data was acquired, hereafter termed GNS II, overlapping with GNS I. The general observing strategy and the reduction pipeline were similar for both surveys, although GNS II used only the H band.

There are two main differences between the two epochs: One is the detector size. In GNS I, the fast photometry mode was

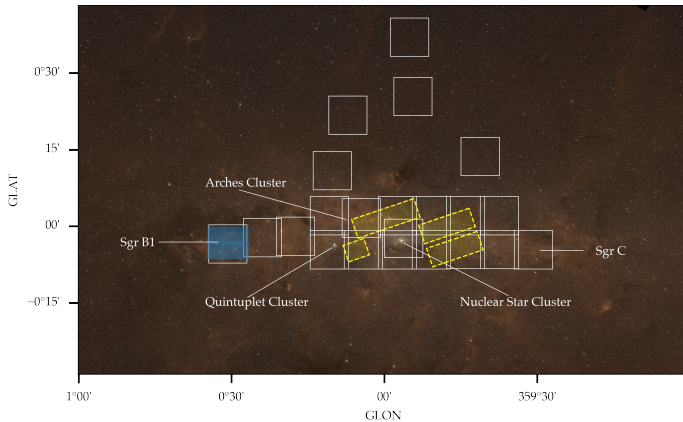


Fig. 1. Coverage of GNS on a Spitzer/IRAC combined mosaic at 3.6, 4.5 and 8 μm (Stolovy et al. 2006). Dashed lines indicate the total coverage of GNS. Solid boxes indicated the areas reduced for this study: white the test field and blue the target field

used, with a DIT of 1.26 seconds, which required using only a third of the detector, i.e. 2048 \times 768 pixels. In GNS II we set a DIT of 3.3 seconds, which allowed us to use the whole chip, 2048 \times 2048 pixels. In Fig. 1 we can appreciate the difference sizes between the pointings. The second difference is the used of Ground-layer adaptive optics assisted by Laser (GRAAL, Paufique et al. 2010) in GNS II. The combination of a longer DIT with adaptive optics resulted in deeper and sharper images.

2.2. Geometric distortions correction

We used SCAMP Bertin (2006) to correct for geometric distortion and to compute the global astrometric solution. A detailed description of the geometric distortion correction process is beyond the scope of this paper; we provide only a summary here.
1. Should I include a link to the pipeline? SCAMP is feed on position catalogs created from each pointing with SExtractor software (Bertin & Arnouts 1996). Then, it computes the global solution by minimizing the squared positional differences between overlapping sources (χ^2_{astrom}) in pairs of catalogs:

$$\chi^2_{\text{astrom}} = \sum_s \sum_a \sum_{b>a} \frac{\|\xi_a(\mathbf{x}_{s,a}) - \xi_b(\mathbf{x}_{s,b})\|^2}{\sigma_{s,a}^2 + \sigma_{s,b}^2} \quad (1)$$

In Eq. 1, s indexes the matched sources, while a and b denote different images. The quantity $\mathbf{x}_{s,a}$ represents the observed position of source s in catalog a , typically in pixel coordinates. The function $\xi_a(\mathbf{x}_{s,a})$ is the transformation that maps these coordinates into a common astrometric reference frame using the current calibration parameters for catalog a . The term $\sigma_{s,a}$ denotes the positional uncertainty associated with source s in catalog a .

In Fig. 2 we show an example of the camera distortion patterns in the HAWKI camera for a data set of GNS2. SCAMP produces an updated header for each of the input images that correct these distortions. Then we apply the correction to the original images and re-project them onto the same grid with SWARP (Bertin et al. 2002).

- Show the quality in astrometry btw GNS1 and 2
- show the quality in photometry

¹ The interested reader can check for example Bouy et al. (2013)

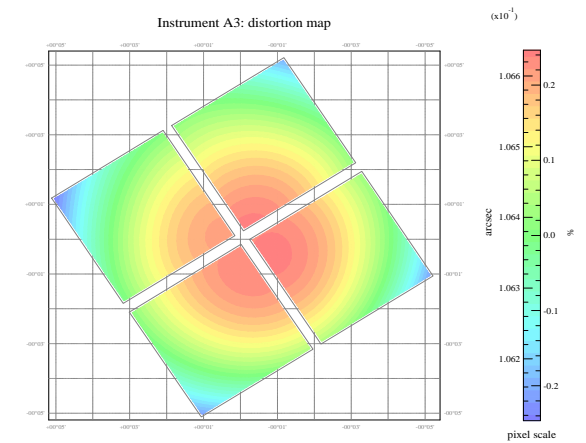


Fig. 2. Example of HAWKI mosaic camera distortion map provided for SCAMP for GNS2 data.

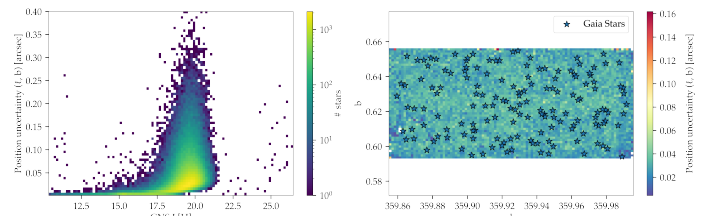


Fig. 3. Astrometric uncertainty. Left: Position uncertainty versus H magnitude for the stars in the solid white square in Fig. 1. Left: Distribution of the position uncertainty across the same field. Black stars mark the position of Gaia stars that we use for proper motions comparison.

2.3. The Proper Motions Catalog

We have reduced an analyzed two different areas and compute proper motions. By applying the holographic technique (Schödel et al. 2013) to the geometric correctec images, we were able to reach a excellent accuracy in photometry and unprecedeted precision in proper motions.

Following we show the main thecnical caratheristcs of the future GNS proper motion catalog (Martínez-Arranz et al. in prep.)

2.3.1. Astrometry

We have reduced te

2.3.2. Proper motion calculations

- Projected coordinates to a common tangential plane
- Projected coordinates of Gaia

The script computes stellar proper motions by matching two catalogs of astronomical sources obtained at different epochs. The procedure is as follows:

The proper motions were computed using two epochs of observations of the same sky region, one from 2015 and the other from 2022. We derived *relative proper motions*, meaning that one epoch (the destination) was chosen as the astrometric reference frame, and the other epoch (the source) was aligned to it.

First, the stellar coordinates from both epochs were projected onto the same tangential plane. Cross-matches were then identified within a small matching radius. A similarity transformation

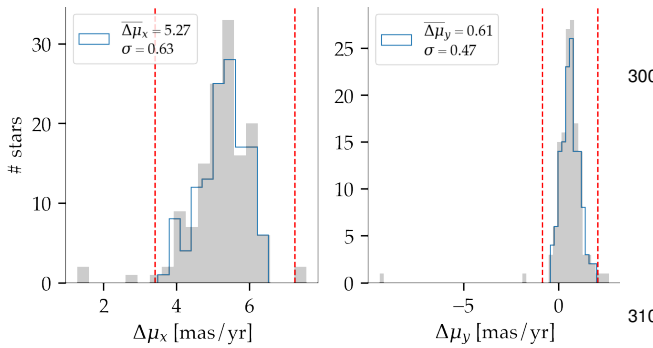


Fig. 4. Gaia-GNS proper motion residuals for the parallel and perpendicular components. Red dashed lines indicate the 3σ level of the distribution. Grey histogram represents the whole set of matches. Blue histogram represent the 3σ clipped distributions

was computed from the matched sources and applied to the entire source catalog. The catalogs were cross-matched again, and a first-degree polynomial transformation was determined from the new matches and applied to all sources. This process was iteratively repeated until the number of matches stabilized or decreased.

Subsequently, the polynomial degree was increased to two, and the iterative alignment procedure was repeated. The same steps were then performed with a third-degree polynomial, resulting in the final aligned catalogs. The positions in the final (transformed) source catalog were compared to those of the destination catalog, and the positional differences were divided by the time baseline between epochs to obtain the proper motions.

Finally, we compared our proper motions with the Gaia stars for DR3 (Gaia Collaboration et al. 2023). We projected the position and velocities of Gaia stars to the same tangential. For the set of Gaia stars, we performed a quality cut: i) We avoided Gaia stars with magnitudes fainter than $G = 19$ and brighter than 13, to prevent high astrometric uncertainties; ii) We discarded Gaia stars with a close Gaia companion to avoid mismatching; iii) We selected only sources with a 5-parameter astrometric solution (position, parallax, and proper motion); and iv) We eliminated Gaia sources with negative parallax, which is unphysical. We refer to the remaining Gaia stars after this quality cut as the reference stars.

In Fig. 4 we show the Gaia-GNS proper motion residuals. After clipping the outliers we reach a level of agreement of 0.6 mas/yr in the parallel component and 0.5 mas/yr in the perpendicular

- Bertin, E. 2006, in Astronomical Society of the Pacific Conference Series, Vol. 351, Astronomical Data Analysis Software and Systems XV, ed. C. Gabriel, C. Arviset, D. Ponz, & S. Enrique, 112
 Bertin, E. & Arnouts, S. 1996, A&AS, 117, 393
 Bertin, E., Mellier, Y., Radovich, M., et al. 2002, in Astronomical Society of the Pacific Conference Series, Vol. 281, Astronomical Data Analysis Software and Systems XI, ed. D. A. Bohlander, D. Durand, & T. H. Handley, 228
 Bouy, H., Bertin, E., Moraux, E., et al. 2013, A&A, 554, A101
 Cano-González, M., Schödel, R., & Nogueras-Lara, F. 2021, A&A, 653, A37
 Clark, J. S., Lohr, M. E., Najarro, F., Patrick, L. R., & Ritchie, B. W. 2023, MNRAS, 521, 4473
 Dong, H., Wang, Q. D., Cotera, A., et al. 2011, Monthly Notices of the Royal Astronomical Society, 417, 114
 Gaia Collaboration, Vallenari, A., Brown, A. G. A., et al. 2023, A&A, 674, A1
 Gallego-Cano, E., Schödel, R., Nogueras-Lara, F., et al. 2020, A&A, 634, A71
 GRAVITY Collaboration, Abuter, R., Amorim, A., et al. 2020, A&A, 636, L5
 Habibi, M., Gillessen, S., Pfuhl, O., et al. 2019, ApJ, 872, L15
 Kruijssen, J. M. D., Longmore, S. N., Elmegreen, B. G., et al. 2014, MNRAS, 440, 3370
 Launhardt, R., Zylka, R., & Mezger, P. G. 2002a, A&A, 384, 112
 Launhardt, R., Zylka, R., & Mezger, P. G. 2002b, A&A, 384, 112
 Libralato, M., Lennon, D. J., Bellini, A., et al. 2021, MNRAS, 500, 3213
 Lu, J. R., Do, T., Ghez, A. M., et al. 2013, ApJ, 764, 155
 Martínez-Arranz, Á., Schödel, R., Nogueras-Lara, F., Hosek, M. W., & Najarro, F. 2024a, A&A, 683, A3
 Martínez-Arranz, Á., Schödel, R., Nogueras-Lara, F., et al. 2024b, A&A, 685, L7
 Matsunaga, N., Kawadu, T., Nishiyama, S., et al. 2011, Nature, 477, 188
 Morris, M. & Serabyn, E. 1996, ARA&A, 34, 645
 Nishiyama, S., Nagata, T., Tamura, M., et al. 2008, ApJ, 680, 1174
 Nogueras-Lara, F. 2022, A&A, 668, L8
 Nogueras-Lara, F. 2024, arXiv e-prints, arXiv:2401.07900
 Nogueras-Lara, F., Gallego-Calvente, A. T., Dong, H., et al. 2018, A&A, 610, A83
 Nogueras-Lara, F., Schödel, R., Gallego-Calvente, A. T., et al. 2019a, A&A, 631, A20
 Nogueras-Lara, F., Schödel, R., Gallego-Calvente, A. T., et al. 2020, Nature Astronomy, 4, 377
 Nogueras-Lara, F., Schödel, R., Najarro, F., et al. 2019b, A&A, 630, L3
 Nogueras-Lara, F., Schödel, R., & Neumayer, N. 2021, A&A, 653, A133
 Nogueras-Lara, F., Schödel, R., & Neumayer, N. 2022, Nature Astronomy, 6, 1178
 Paufique, J., Bruton, A., Glindemann, A., et al. 2010, in Society of Photo-Optical Instrumentation Engineers (SPIE) Conference Series, Vol. 7736, Adaptive Optics Systems II, ed. B. L. Ellerbroek, M. Hart, N. Hubin, & P. L. Wizinowich, 77361P
 Paumard, T., Genzel, R., Martins, F., et al. 2006, ApJ, 643, 1011
 Portegies Zwart, S., Makino, J., McMillan, S., & Hut, P. 2001, The Astrophysical Journal, 565
 Schödel, R., Yelda, S., Ghez, A., et al. 2013, MNRAS, 429, 1367
 Schonrich, R., Aumer, M., & Sale, S. E. 2015, The Astrophysical Journal, 812, L21
 Shahzamanian, B., Schödel, R., Nogueras-Lara, F., et al. 2019, A&A, 632, A116
 Shahzamanian, B., Schödel, R., Nogueras-Lara, F., et al. 2022, A&A, 662, A11
 Sormani, M. C., Sanders, J. L., Fritz, T. K., et al. 2022, MNRAS, 512, 1857
 Stolovy, S., Ramirez, S., Arendt, R. G., et al. 2006, in Journal of Physics Conference Series, Vol. 54, Journal of Physics Conference Series, ed. R. Schödel, G. C. Bower, M. P. Munoz, S. Nayakshin, & T. Ott (IOP), 176–182

3. Results

- Compare with Hosek
- Compare with Libralato
- Compare with Gaia

4. Conclusions

Discussion and conclusions.

References

- Bartko, H., Martins, F., Trippe, S., et al. 2010, ApJ, 708, 834
 Beroiz, M., Cabral, J. B., & Sanchez, B. 2020, Astronomy and Computing, 32, 100384